Journal of Membrane Science 618 (2021) 118657

Contents lists available at ScienceDirect

Journal of Membrane Science

journal homepage: http://www.elsevier.com/locate/memsci

Elucidating the roles of diffusion and osmotic flow in controlling the geometry of nanochannels in asymmetric track-etched membranes

I.V. Blonskaya [a], N.E. Lizunov [a], K. Olejniczak [a,b], O.L. Orelovich [a], Y. Yamauchi [a], M. E. Toimil-Molares [c], C. Trautmann [c,d], P.Y. Apel [a,e,*]

[a] Flerov Laboratory of Nuclear Reactions, Joint Institute for Nuclear Research, Joliot-Curie Str. 6, 141980, Dubna, Russia
[b] Nicolaus Copernicus University, Gagarina Str. 7, 87-100, Torun, Poland
[c] GSI Helmholtzzentrum für Schwerionenforschung GmbH, 64291, Darmstadt, Germany
[d] Materialwissenschaft, Technische Universität Darmstadt, Alarich-Weiss-Straße 2, 64287, Darmstadt, Germany
[e] Dubna State University, Universitetskaya Str. 19, 141980, Dubna, Russia

ARTICLE INFO

Keywords:
Track etching
Asymmetric membranes
Electrical conductance
Osmosis
Viscous flow

ABSTRACT

Asymmetric membranes and asymmetric pores are broad classes of objects, the role of which is steadily growing in academia and industry. During the last two decades, asymmetric (often called "conical") track-etched nanopores have attracted increasing attention from the scientific community due to their great potential for accomplishing useful functions in nanofluidic devices. A great body of knowledge has been gained on the electrical and electroosmotic properties of track-etched asymmetric nanopores in electrolyte solutions. Less attention has been paid to the pore geometry, and practically no attempts have been made to explore their osmotic and hydraulic properties. The present study fills this gap by examining the interrelations between the electrical, osmotic, hydraulic and structural characteristics of an asymmetrically etched ion-track nanopore. Several consecutive phases of pore evolution are identified. In the last phase, the highly asymmetric membrane resembles a porous 2D material. The temporal dependences of the two counter-fluxes – the diffusional flux of the etchant and the volume flux of stopping media - are elucidated and analyzed in light of their effect on the nanopore configuration. The osmotic reflection coefficients of highly asymmetric pores are estimated under etching conditions and in diluted electrolyte solutions. Our results allow a new level of understanding of the phenomena underlying the development of an ion-track nanopore and pave the way for the controlled fabrication of a variety of nanopores of different shapes using one and the same principle of an asymmetric chemical treatment.

1. Introduction

Asymmetric membranes and asymmetric pores are broad classes of objects, the role of which is steadily growing in academia and industry. Asymmetric membranes play an extremely important role in diverse branches of membrane technology, including reverse osmosis and nanofiltration [1], ultrafiltration and microfiltration [2,3], and membrane distillation [4]. Especially important are asymmetric membranes with a thin selective layer, which provide high performance in pressure-driven and osmotic driven separation processes [5–8]. Another rapidly growing field is the development of biomimetic sensors based on molecularly imprinted membranes [9]. Due to the demand of sensor technology over the last three decades, there has been growing interest in nanoporous membranes and in particular, nanopores. Depending on the material and fabrication method, nanopores can be divided into two large categories, namely, biological nanopores and solid-state nanopores [10–12]. The former are natural protein ion channels created by molecular self-assembly in a cell lipid membrane, which have precisely determined diameters typically ranging from 1 to 4 nm, such as α-hemolysin [12], and other pore-forming proteins [10,11,13,14]. The latter are artificially fabricated pores in solid-state membranes, such as silicon nitride [15], silicon oxide [16], graphene [17], molybdenum disulfide [18], or polymer [19] by using the following techniques: focused ion beam [20], electron beam [21], electrochemical etching [22], monomer seeding [19] and bombardment with high-energy heavy ions followed by wet etching [23,24] or aqueous extraction processing [25].

* Corresponding author. Flerov Laboratory of Nuclear Reactions, Joint Institute for Nuclear Research, Joliot-Curie Str. 6, 141980, Dubna, Russia.
E-mail address: apel@jinr.ru (P.Y. Apel).

https://doi.org/10.1016/j.memsci.2020.118657
Received 23 June 2020; Received in revised form 19 August 2020; Accepted 20 August 2020
Available online 31 August 2020

Moreover, researchers have tried to insert a biological nanopore into a solid-state pore [26,27] and have obtained so-called hybrid nanopores to combine advantages inherited from both [28]. Apart from sensing techniques, nanopores have been widely explored for the purposes of basic science and for use in a broad range of applications, including studies on the hindered transport of ions and molecules, ion separation, nanofluidics, energy harvesting, and others.

Among the asymmetric membranes and asymmetric nanopores, those produced using the track etching method deserve special attention [24,29,30]. A unique feature of the track etching technique is the possibility of fabricating membranes with a predetermined number of pores, including single nanopore membranes [31]. Both multi- and single-pore asymmetric track-etched membranes (ATEMs) are employed to study the ion transport phenomena in restricted volumes [32–36], to build functional nanofluidic devices, such as molecular sensors [32, 35–40], pumps and gates [41–43], logical elements [40,42,44], and others. Based on asymmetric track-etched nanoporous membranes, highly efficient ion separation and osmotic energy harvesting processes were recently suggested [45,46]. An inherent property of ATEMs is the electric surface charge, with an isoelectric point of approximately 3.8 [47]. Due to their surface charge and geometrical asymmetry, ATEMs exhibit ionic current rectification in electrolyte solutions, which is the basis of many potential applications. Sensor applications of asymmetric track-etched nanopores are based either on diode-like properties [35–37,40] or the resistive pulse principle [32,38,39], also called steady-state and transient-state sensing, respectively [24]. The performance of asymmetric nanopores as sensors critically depends on the pore geometry, especially on the shape and size of their tips.

All the ATEMs employed in the above listed studies are obtained using either one-sided (also referred to as asymmetric) etching [47] or surfactant-controlled etching [48] of ion tracks in polymer foils. Both methods are well known and proven to be efficient tools that allow the fabrication of highly asymmetric channels with openings on the nanometer scale at one end (the so-called pore tip) and approximately two orders of magnitude larger openings (called bases) at the other end. The advantages and shortcomings of both methods are discussed in Ref. [30]. To date, the former method is more popular, especially when single pores are produced. Briefly, the method involves the irradiation of a polymer foil with accelerated ions and further etching from one side with a strong etchant solution, while the other side of the foil faces a stopping solution. Despite the wide applicability of this procedure, many aspects concerning the mechanism of asymmetric etching and the exact geometry of the resulting channels are still not well understood. Recently, the process of asymmetric etching of ion tracks in polyethylene terephthalate films was subjected to a more rigorous analysis, and some new phenomena were identified [49,50]. Particularly, it was found that asymmetric etching conditions generate osmotic flow through an ion-track pore and that the ratio between the osmotic water flux and the diffusional alkali flux is a factor affecting the pore geometry. However, the temporal development of the counter-fluxes of water and solute during the osmotic process and the values of the reflection coefficients that characterize the osmotic properties of the pore tip remain unknown.

The goal of this work is to better understand the physical and chemical phenomena accompanying the asymmetric etching of ion tracks in polymer foils. We will focus on what occurs after the etchant and stopping solutions meet each other in a newborn nanochannel and what new potentialities for controlling the nanopore geometry and its functions can be identified. The detailed knowledge of the nanopore geometry is needed with regard to all existing and potential applications of asymmetric track-etched nanochannels.

2. Experimental

2.1. Polymer foils and ion irradiation

Polyethylene terephthalate (PET) biaxially oriented, semicrystalline, 12-μm-thick films (Hostaphan RN, Kalle, Germany, or Hostaphan RNK12, Mitsubishi Polyester Films, Germany) were irradiated with single and multiple (fluences of 10^7-10^8 cm^{-2}) 2-GeV Au ions at the UNILAC accelerator of GSI (Darmstadt). The actual track densities were determined using field emission electron microscopy (FESEM). Given the large range of Au ions (>130 μm) [49], we irradiated stacks of 7 foils (a total thickness of 84 μm). The specific energy loss of the ions when passing through the foil stack varied only by approximately 10% (18–20 MeV/μm [51]); therefore, one can expect nearly similar etching characteristics of the ion tracks in all foils.

2.2. Sensitization of the ion tracks prior to etching

Samples of the ion-irradiated films were exposed for 60 min to ultraviolet (UV) radiation of LE-30 lamps (Lisma, Saransk, Russia) in air using a pristine PET film as a filter. The intensities measured by a TPK-PKM radiometer were 3–4 W/m^2 in the UVA range (315–400 nm) and ~1 W/m^2 in the UVB range (280–315 nm). The suppression of radiation at a wavelength of <315 nm by the PET filter provided conditions under which photo-oxidation occurs mostly in the ion tracks and does not damage the polymer.

2.3. Asymmetric etching of single tracks

The asymmetric etching of single-track samples was performed in a two-compartment electrolytic cell [47], see Fig. 1A. One compartment was filled with 9 M NaOH, and the other compartment contained a stopping solution. Different stopping solutions were used, including water and a mixture of 2 M KCl and 2 M HCOOH (50:50, v/v), referred to as 1 M KCl/1 M HCOOH throughout the paper. Conductometric monitoring of the etching process was performed in DC mode using a PC-controlled Keithley 6482 picoammeter (Keithley Instruments, Cleveland, OH). A bias voltage of 1 V was applied to the gold electrodes (1 cm^2 surface area), always with a positive sign on the alkali side. The electrodes must be able to withstand many repeated experiments, thus, to be robust enough, these electrodes were fabricated from a wire with a diameter of 2 mm. All experiments with single track samples were performed in a Friocell Refrigerated Incubator (Fisher Scientific) at a temperature of 22.0 ± 0.2 °C.

Ultra-pure water, 18.2 MOhm·cm, from Arium (Vladisart) and reagent grade chemicals from Sigma Aldrich were used for solution preparation.

2.4. Asymmetric etching of multitrack samples

To observe and measure the osmotic flow through newborn pores in PET foils during asymmetric etching, the cell was equipped with a fluoropolymer capillary with a 2-mm inner diameter [49]. The capillary was inserted into the compartment with the alkaline solution (see Fig. 1B). Platinum wires with a diameter of 0.5 mm (i.e. much smaller than the diameter of the capillary) were used as electrodes. The total area of the sample was 2.8 cm^2; however, only a central circle of 1 cm^2 was sensitized with UV light, as described previously [49]. The tracks in the sensitized area are etched much more rapidly than the nonsensitized tracks outside the circle. This avoided disturbances caused by the “edge effects” of the air bubbles and mechanical strain on track etching. The inner volume of each compartment of the cell was 3 cm^3. All etching experiments were performed in a temperature-conditioned room at 22–23 °C. Conductometric monitoring of the etching process was performed in AC mode using a PC-controlled LCR meter (HiTESTER-3522-50, HIOKI E. E. Corporation, Japan) [49]. To avoid

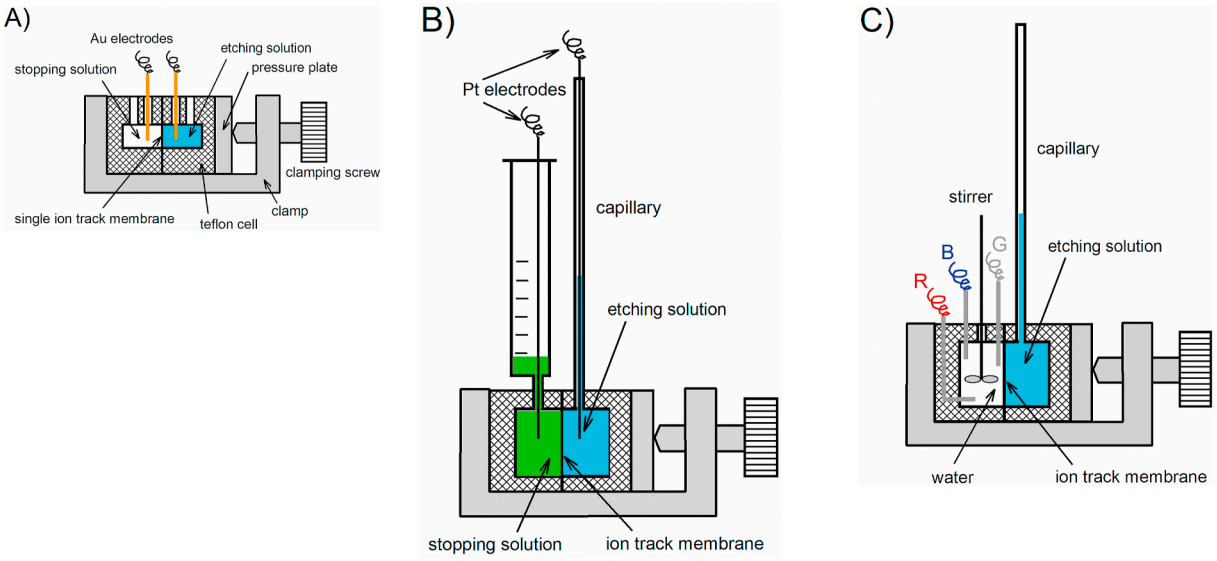

Fig. 1. The cells used to study the asymmetric etching of ion tracks in PET foils. A: Single-track etching with conductometric monitoring. B: Multitrack etching with a parallel measurement of osmotic flow and monitoring of the ionic current through the membrane. C: Multitrack etching with a parallel measurement of osmotic flow and conductometric monitoring of the sodium hydroxide concentration in the stopping solution.

polarization of electrodes, a sinusoidal voltage of 0.5 V at a frequency of 1333 Hz was applied to the wire electrodes.

The osmotic flux of water through the membrane was calculated from an increase in the etchant solution volume in the measuring capillary. The actual volume of water is several percent larger than the change in the solution volume because of the difference between the partial molar volumes of pure water and water in a strong alkali solution [52]. This phenomenon was taken into account.

The other mode of multitrack etching was accomplished using the cell shown in Fig. 1C. The alkaline compartment of the cell is also equipped with a Teflon capillary, while the compartment of the stopping solution is equipped with three platinum wire electrodes - R, G and B - placed at different distances from the membrane. The stopping solution, namely, deionized water, was stirred with a small propeller to equalize the alkali concentration, which comes through the membrane, throughout the compartment. For better accuracy, the quantity of water was determined by weighing. The measurement of three resistances – between R and G, G and B, and R and B – allowed us to ensure that the alkali was homogeneously distributed in the compartment. Calibration experiments with NaOH solutions of different concentrations were performed to build the calibration curve needed to determine the alkali concentration as a function of time from the resistance measurements. Since the resistance ranged up to relatively low values, a higher frequency (40 kHz) was needed to avoid errors caused by the polarization of the electrodes. To avoid heating of the solution, a low voltage (0.2 V) was applied.

2.5. SEM studies of etched multipore samples

After the etching process was stopped, the samples were rinsed with deionized water and air-dried. Electron microscopy investigations were performed on the multitrack samples using a field emission electron microscope (Hitachi SU8020, Japan). The surface of the samples was sputter-coated with a 10-nm-thick Au–Pd layer. The geometry of the pores was determined by imaging the cross section of the fractured samples. A photo-oxidation technique based on a long exposure to soft UV radiation was employed to render the initially viscoelastic polymer films brittle [48–50]. Ninety percent of the UV exposure was applied to the base side, and only 10% was applied to the tip side of a sample to be fractured. This precaution was needed to prevent the ablation and distortion of the thin layer with small pore openings.

3. Results and discussion

3.1. Asymmetric etching of single- and multitrack samples. Correlation among the ionic conductivity, osmotic flow and pore geometry

Fig. 2 shows the temporal dependence of three important characteristics monitored during asymmetric etching. The ionic current through a multitrack sample, osmotic flow through the multitrack sample and ionic current through three typical single-track samples are presented as functions of time. From a comparison of the ionic currents shown in panels A and C, one can conclude that, obviously, there are no through-etched pores in the multitrack sample for the first ~ 60 min. However, the ionic current slowly increases during this time interval, reaching a value of approximately $5{\cdot}10^{-2}$ μA ($5{\cdot}10^{-8}$ A). Since the number of tracks is ~ 10^7, the average current through an individual track is as low as ~ 10^{-14} A. The latent tracks soaked with water are slightly electroconductive [53–55], and their conductivity slowly increases. Apart from the soaking and diffusion of ionic species into a track, the extraction of radiolysis and photo-oxidation products, first of all the terephthalic and hydroxyterephthalic acid anions, from tracks can contribute to the growing conductivity [56]. Furthermore, between 60 min and approximately 110–120 min, the process of pore opening causes a considerable increase in the ionic current through the multitrack sample by more than 4 orders of magnitude. Single tracks showed the breakthrough times within this time interval: 65, 77 and 90 min (Notably, compared to previous similar experiments [49], the etching of both single and multiple tracks occurs faster due to a higher UV intensity and thus a stronger sensitization of the tracks). The process of gradual pore opening and the formation of an array of pores that do not generate osmotic flow is denoted as stage II in Fig. 2. At 120 min, the current through the multitrack sample reaches ~ 10^{-3} A. A typical current through a single track in this period of time is ~ 10^{-10} A, as seen in panel C. One can conclude that there is a reasonable proportionality between the ionic currents through one pore and 10^7 pores. Note, however, that the electrical conductivities were measured in different modes, and a direct comparison is not strictly valid. Nevertheless, a good correlation is evident. Measurable osmotic flux through the multitrack sample starts at approximately 120 min, i.e., considerably later than the breakthrough time of the majority of pores. The shift in time between the pore opening and the development of osmotic flow will be discussed below. As to the further development of the ionic current through the membrane, its

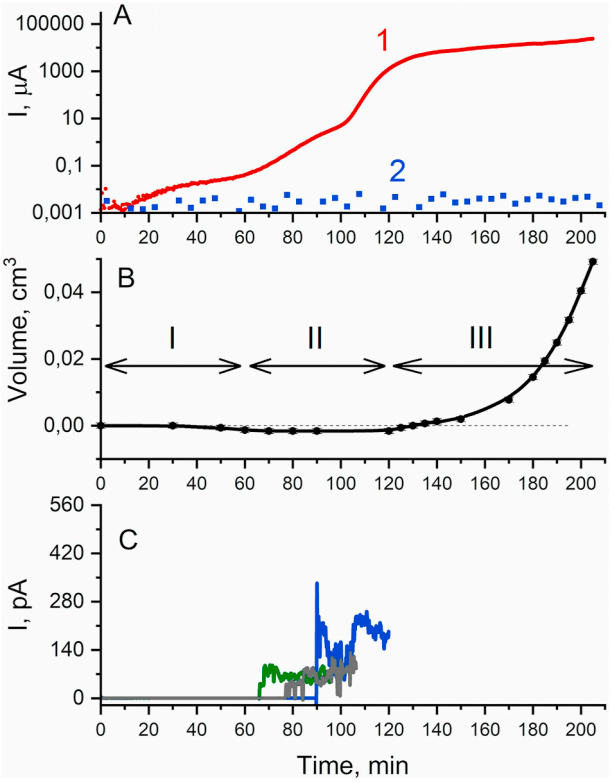

Fig. 2. Asymmetric etching of single- and multitrack samples. Panels A and B: Multitrack sample (Hostaphan RN, Au ions, $1.3{\cdot}10^7$ cm^{-2}). A: Curve 1 is the ionic current through the membrane measured in AC mode (voltage of 0.5 V) as a function of time; the series of points (labeled 2) are the background measured under the same conditions with a nonirradiated foil. B: The volume of osmotically pumped water as a function of time. Panel C: Three independent etching experiments with single tracks. Ionic current measured in DC mode at 1 V, as a function of time. Each was conducted for 30 min after breakthrough. Etchant: 9 M NaOH. Stopping solution: 1 M KCl/1 M HCOOH. Three stages of the multitrack etching process are indicated in panel B: I – no through pores in the membrane; II – the pore opening process and the formation of an array of approximately conical pores; and III – the development of osmotic flow due to the transformation of the pore geometry.

increase after 120 min slows down because the resistance of solutions in the cell limits the current. We did not correct the measured ionic current by subtracting the cell resistance from the total resistance because the former is not constant, and this procedure would yield misleading results.

The delay between the formation of the through pores and the measurable osmotic flow suggests that the model presented in Ref. [49] should be revised. It is clear that the newborn through pores do not show pronounced osmotic effects, while the pores that underwent a certain evolution do generate osmotic flow. Let us analyze the situation in light of the data available on cylindrical track-etched nanopores that are 20–50 nm in diameter and inorganic salt solutions [57]. It has been shown that osmotic phenomena are caused merely by ionic selectivity of the negatively charged nanopores. It is unlikely that the newborn asymmetric pores possess a lower ionic selectivity compared to those that were subject to continued etching. Rather, hydraulic resistance can be regarded as the decisive factor in the temporal development of osmotic flow. The gradual evolution of the pore shape with the increasing time of asymmetric etching was illustrated by a series of FESEM images in Ref. [50]. Below, we show a set of new micrographs selected from a large array of images taken both for Hostaphan RN and Hostaphan RNK foils. To make the results more representative and general, we analyzed two types of PET foils that are similar to each other with regard to most properties but slightly differ by morphology and distribution of inorganic filler particles across the thickness [58].

Fig. 3A shows a typical shape of a pore that has not yet broken through the entire thickness of the foil. In terms of the classification given in the legend of Fig. 2, this image corresponds to stage I. FESEM images in Fig. 3C and E shows pore tips soon after breakthrough and correspond to stage II of the multitrack etching process. We clearly see an elongated narrow pore tip both in Fig. 3B and especially in Fig. 3C, the origin of which is cross-linking in the track halo, as has been explained in detail in previous publications [30,49]. From Fig. 3C, one can easily find that the narrowest pore segment with a length $L \approx 1$ μm is nearly a cylinder (cone angle $2\alpha \leq 0.5°$) with a diameter $d \approx 15$ nm. The dimensions were measured at an appropriate magnification of the image. Narrow cylindrical channels have a high resistance to viscous flow, in accordance with the Poiseuille equation [59]:

$$Q_{cyl} = \frac{\pi d^4 \Delta P}{128 \mu L} \tag{1}$$

where Q_{cyl} is the volume flux at a pressure difference ΔP and μ is the viscosity of the liquid.

At stage III, as seen in Fig. 3F and H, the pore tips acquire completely different configurations. The narrowing becomes very short, still keeping its small diameter. The geometry of the pore tip approaches the case of a circular aperture in a plane wall for which the formula for the volume flux Q_{ap} is [60]:

$$Q_{ap} = \frac{d^3 \Delta P}{24 \mu} \tag{2}$$

It has been shown in Ref. [57] that osmotic flow generated by a salt concentration difference along a track-etched cylindrical nanochannel obeys the Poiseuille law for viscous flow, and therefore, we can use (1) and (2) to predict osmotic fluxes through asymmetric pores at stages II and III. The ratio k between the viscous fluxes for these two cases is

$$k = \frac{Q_{ap}}{Q_{cyl}} = \frac{16L}{3\pi d} \tag{3}$$

It is assumed that the driving force (ΔP or osmotic pressure $\Delta \Pi$) is similar for both pores. Taking $d = 15$ nm and $L = 1000$ nm, we determine that the pore tip shown in Fig. 3C has 113 times higher hydraulic resistance than an aperture with the same diameter in an infinitely thin wall. Therefore, a decrease in the hydraulic resistance should be the main reason for the rapid development of osmotic flow in stage III. Note that the tips in stage III remain narrow enough to possess a certain ionic selectivity and a nonzero reflection coefficient.

Two pairs of images - Fig. 3B and C and Fig. 3D and E - look very similar; however, a small but significant difference between them deserves a special comment. The pores in Fig. 3D and E have a nearly ideal conical geometry. By chance, the etching was stopped at the moment when the pores had this shape. Before this moment, the pores had a funnel-like shape, as shown in Fig. 3B and C. Further etching will change the conical pore geometry toward the configuration shown in Fig. 3F and H. In numerous experimental works, researchers use a formula for the electrical resistance of a conical conductor to find the tip radius of asymmetric track-etched pores from their conductivity data. However, the FESEM observations and dynamic conductivity measurements [49] show that the "conical" approach is justified only in rare cases (an example is Fig. 3D). In most situations, it is not known exactly at what stage of pore evolution the asymmetric etching was stopped, and therefore, the mentioned approach may lead to either an underestimated or overestimated tip radius.

The evolution of the pore tip in stages II and III can be qualitatively explained from Fick's first law. The alkali diffusion flux J along the pore of an arbitrary shape, including the conical one, is given by

$$J = -\pi D r^2 \frac{dc}{dx} \tag{4}$$

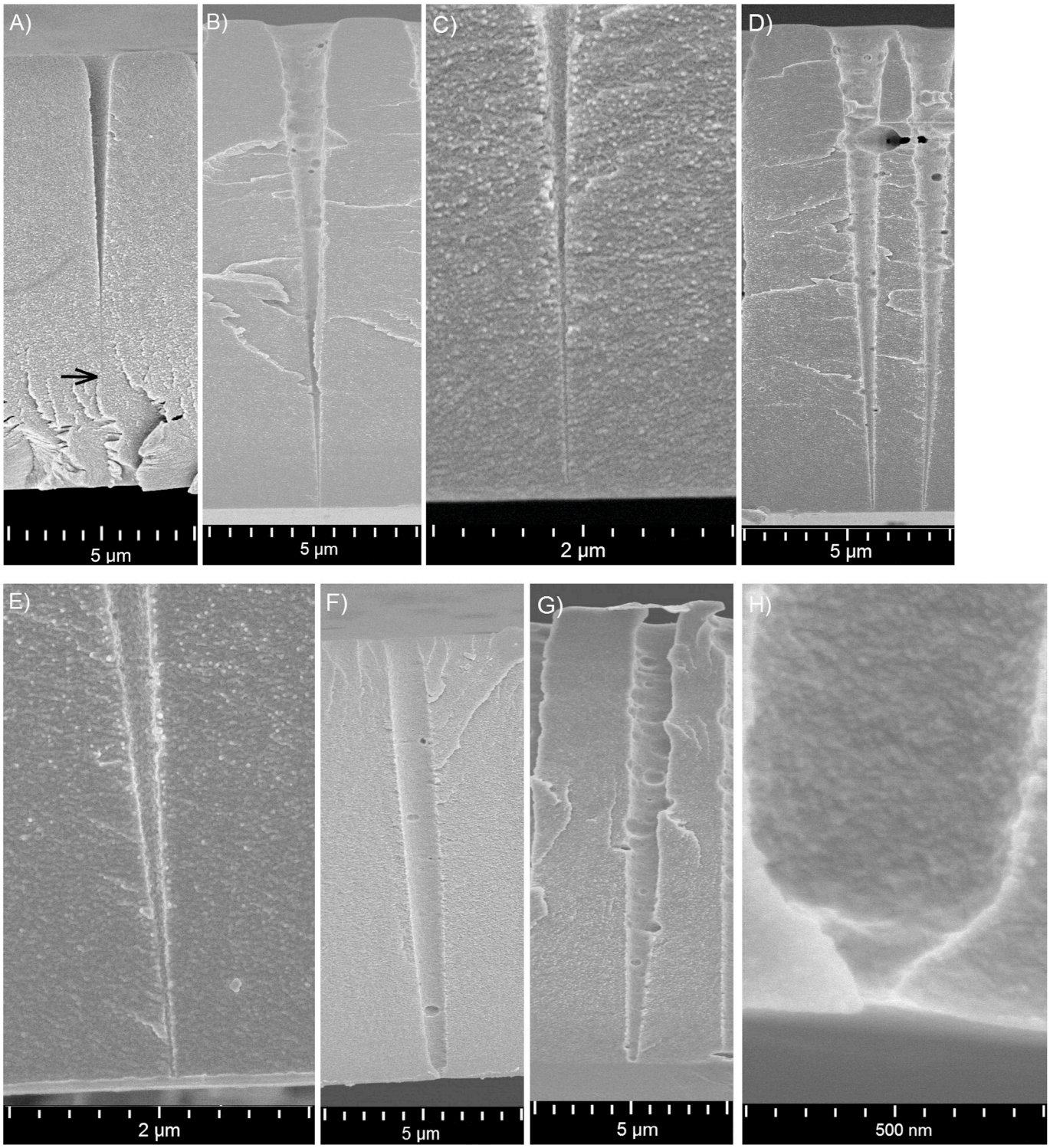

Fig. 3. Asymmetric pores at different stages of etching. Stage I: Image A. Stage II: Images B, C, D, E. Stage III: Images F, G, H. PET foils (A, F, H: Hostaphan RNK12; B, C, D, E, G: Hostaphan RN12) irradiated with multiple Au ions. A: a pore that has not yet etched through the foil. The arrow points to where the track is still visible. B, D. F, G: whole pores. C, E, H: pore tips. Image G illustrates the membrane from the experiment shown in Fig. 2. All other pores are obtained using 9 M NaOH as the etchant and water as the stopping solution.

where D is the diffusion coefficient, r is the pore radius, x is the distance along the pore, and c is the alkali concentration. At equilibrium, the flux J is constant, and equation (4) can be written as

$$\frac{dc}{dx} = -\frac{J}{\pi D r^2} \tag{5}$$

In a tapered pore with $r = r(x)$, the concentration gradient is substantially nonlinear and is a maximum at the smallest r, i.e., in the pore tip region. For this reason, the shape of a pore that initially was approximately conical rapidly changes. The angle of the taper of the pore tip increases, and finally, an asymmetric membrane with a selective skin layer forms. Therefore, the conditions for observable osmotic flow

are fulfilled.

3.2. Asymmetric etching of multitrack samples. Measurements of the counter-fluxes of water and alkali through the pore tip

Fig. 4 illustrates the results of experiments aimed at studying the correlation between the pore opening process and the development of the counter-fluxes of the solution components through the pores. Panel A shows the concentration of alkali that diffused into the stopping solution, i.e., water, and the volume of water osmotically pumped into the etching solution, curves 1 and 2, respectively. Panels B, C and D show three records "ionic current vs. etching time" for the single tracks. Typical breakthrough times are shorter than the case with 1 M KCl/1 M HCOOH as the stopping solution. This effect of the acidity of the stopping solution was observed and interpreted previously [49,50]. Another feature of the process is the very low conductance of a nanopore. A typical current is several units of pA at the moment of breakthrough and reaches a level of 100 pA in ~ 1 h. With water as the stopping solution, only cations from the etching solution, Na^+, can contribute to the ionic current in DC mode. There are no anions that could be dragged through the pore and cause the electrical current.

Similar to Fig. 2, the stage of through pore formation is not accompanied by osmotic flow (see curve 2 in panel A). A measurable osmotic flux starts after the pores have undergone considerable evolution due to continued asymmetric etching. The absolute value of the alkali diffusion flux into the stopping solution is also low at the beginning of stage II and increases toward the end of this stage. The channels with long and narrow tips constitute a high resistance to diffusion. When the pore tips approach the geometry shown in Fig. 3H, both the osmotic flow and the growth of alkali concentration in stopping solution accelerate considerably.

Interestingly, the alkali concentration in the stopping solution (curve 1 in panel A of Fig. 4), which is as high as 0.1–0.5 mol/L, does not suppress the osmotic flow. This result indicates that the reflection coefficient of the nanopores is not zero despite the thickness of the electrical double layer is very small (<1 nm) on both sides of the membrane.

The measured quantities as functions of the time t – [NaOH] and V_{meas} – were used to calculate the counter-fluxes of water and sodium hydroxide. When treating the experimental data, the following points were taken into account:

- The partial molal volume of water decreases when it is added to 9 M NaOH (a molality of 9.54 mol kg^{-1} at 20 °C). Therefore, a correcting coefficient of 1.06 was used to calculate the true volume of water $V(t)$ from an increase in the etching solution volume $V_{meas}(t)$ [52].
- When alkali molecules leave the etchant solution, its volume decreases according to the apparent partial molal volume $\phi = 6.3$ cm^3/mol [52] of sodium hydroxide in the solution of the above molality. Therefore, the product of ϕ and the alkali flux was added to V_{meas}.
- The contribution of a small admixture of etching products to the conductivity of the stopping solution was neglected.

The calculations yield the plot shown in Fig. 5. The alkali flux (curve 1) starts to grow in the middle of stage II but declines in the middle of stage III. In the beginning of stage III, water and alkali ions move toward each other in nearly equal molar quantities. Their ratio (curve 2) grows upon the development of the osmotic flow and reaches a factor of ~4 by the end of the experiment. The estimates are not reliable for times less than 100 min because of the low values of volume flow through the membrane. Fig. 5 is a clear demonstration of the direct influence of the pore configuration on the proportion between the counter-fluxes of the two solution components. As the pore channel widens, the diffusional flux J should grow proportionally to the area of the cross section. Assuming that the pore radius increases linearly with time in any region of the channel, we should expect that the diffusional flux is proportional to time squared. The viscous flux of solvent Q_s grows in the same region as the 4th power of time (via the factor d^4 in the Poiseuille equation). Therefore, the ratio Q_s/J should grow superlinearly with time, and this conclusion is supported by our experimental results. Of course, the above reasoning is a very simplified description because the driving forces of the two counter-fluxes may change in time and not in a symbiotic manner.

The linear velocity v of the solution moving through the tip is also of interest. This quantity can be calculated if the tip radius is known. Based on the estimates of the tip radius given in Section 3.4, the linear velocity by the end of stage III is found to be equal to 0.17 cm s^{-1}. In stage II, when the osmotic flux has not yet shown up, values of v are orders of magnitude lower. Note that for the acidic stopping solution (Fig. 2), the osmotic flow, normalized to one pore, grows more rapidly. This has been reported earlier [49,50], and the same conclusion can be made from a comparison of Figs. 2 and 4. Assumingly, a higher concentration polarization suppresses the osmotic flow in the case of a neutral stopping

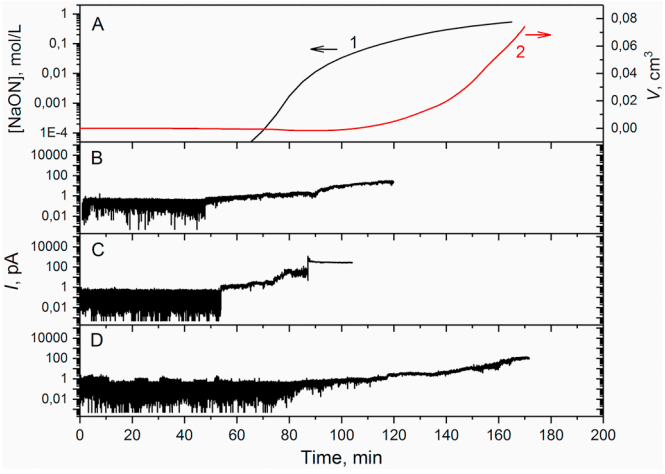

Fig. 4. Panel A: Asymmetric etching of a multitrack sample (Hostaphan RNK12, Au ions, $8 \cdot 10^7$ cm^{-2}). 1: alkali concentration [NaOH] in stopping solution as a function of time; 2: volume V of osmotically pumped water as a function of time. Panels B, C and D: Three independent etching experiments with single tracks. Ionic current measured in DC mode at 1 V as a function of time. Etchant: 9 M NaOH. Stopping solution: pure water.

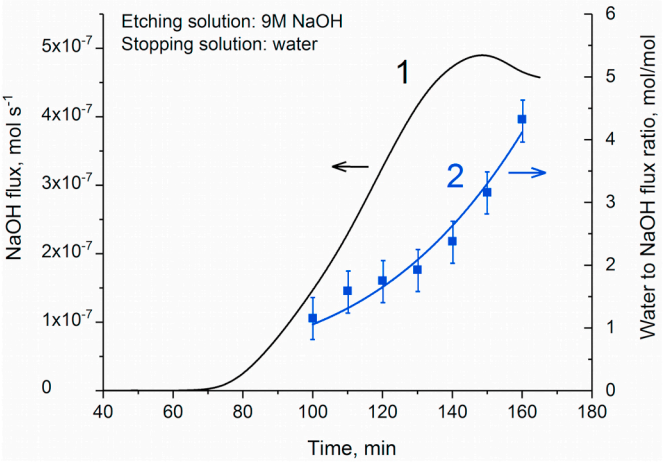

Fig. 5. The diffusion flux of the alkali (1) and the ratio between the osmotic flux of water and the diffusion flux of the alkali (2) through the membrane as functions of the time of asymmetric etching. The fluxes are calculated from the experimental data of Fig. 4, panel A. Curve 2 is drawn to guide the eye. The errors are mainly due to an uncertainty in the determination of the solution level in a measuring capillary.

solution. At the end of etching, the osmotic flux per pore is approximately 3 times higher from the 1 M KCl/1 M HCOOH solution than from water. Therefore, the linear velocity of flow from the acidic solution is ~ 0.5 cm s^{-1}, which suggests that the influence of osmotic flow on the alkali concentration gradient in the pore is stronger. These considerable velocities of the volume flow may cause the observed decrease in the diffusion counter-flux of the alkali ions. An exact quantitative analysis of the situation is not possible because of the unknown diffusion coefficients of NaOH in a constrained space and in the presence of etching products.

An additional comment is needed concerning the choice of the stopping solution recipe used in this section. Pure water was employed for two reasons. First, the absence of dissolved electrolytes made it possible to measure small quantities of alkali diffusing from the etching compartment, and, second, prevented nanoprecipitation in pore tips. In contrast, if KCl had been added to the stopping solution, the contaminant nanoparticles adsorbed in the pore lumen could have affected the membrane osmotic and hydraulic properties [49]. For the same reason, the majority of pores imaged in Fig. 3 were obtained with water as the stopping solution. This precaution allowed us to fabricate channels free of any nanoprecipitations, regardless of the time of contact between the etching and stopping solutions.

When considering water transport through the pore, it should be taken into account that a certain quantity of water is produced in the reaction between formic acid and hydroxide ions.

$$HCOOH + OH^- \rightarrow H_2O + HCOO^-$$

in the case when an acidic stopping solution is used. From the FESEM images of magnesium-containing nanocrystals in asymmetric nanopores etched using a neutral stopping solution [49], we can conclude that the majority of nanoprecipitations, caused by impurities in the stopping solution, form outside the pore tip. Thus, the chemical interaction between the alkali and the components of the stopping solution mostly occurs outside the pore. Clearly, the same applies to the neutralization reaction. Based on the concentration gradients, one can expect that the diffusion-driven alkali flux out of the pore is approximately 9 times higher than the diffusion-driven acid flux into the pore. Therefore, the production of water predominately occurs in the stopping solution. A much smaller quantity of water is synthesized inside the pore and this quantity adds to the osmotic water flux, yielding the total build-up of water in the alkaline compartment of the cell. In stage III, acetic acid will also be transported into the pore by convection, and the production of water will increase. This process can play a certain role under the conditions of the experiment shown in Fig. 2(A, B) but is absent under the conditions of the experiment shown in Fig. 4A.

3.3. FESEM studies of the highly asymmetric membrane of Section 3.2

The membrane obtained in the experiment of Fig. 4A was subjected to FESEM examination. The pore openings on the etched side (Fig. 6A) are elliptical. The geometrical mean of the two axes, averaged over several pores, is 1.03 μm. The pore openings on the opposite side (Fig. 6B and C) are so small that many of them could not be measured accurately. To prevent damage to the sample, the examination was performed at an accelerating voltage of 3 kV, which did not allow the highest resolution. Some pores are as large as ~ 50 nm; however, the diameters of most openings are equal to or smaller than ~ 20 nm. The dark halos around the pores in Fig. 6B are signs of the small thickness in these areas. The reason for the wide variation in the opening diameters is the pore channel configuration. Short channels span a thin wall at the pore bottom. The thickness of the wall is comparable with the channel diameter and with the PET crystallite size [58]. Under such conditions, the heterogeneity of the semicrystalline polymer matrix may cause the formation of irregular openings.

3.4. ATEM hydraulic permeability, osmotic properties, reflection coefficient and pore tip size

The experiment shown in Fig. 4A was stopped at 170 min when the osmotic flux Q_s was equal to $2.3 \cdot 10^{-3}$ cm^3 min^{-1}. The height of the alkali solution level was 2.3 cm, which corresponds to a hydrostatic pressure ΔP_s of 0.30 kPa. The sample was carefully washed, and a water flow rate Q was measured at a hydrostatic pressure ΔP of 5.0 kPa. The measurements were repeated for two opposite directions of flow through the asymmetric membrane, and a value of 0.019 ± 0.001 cm^3 min^{-1} was

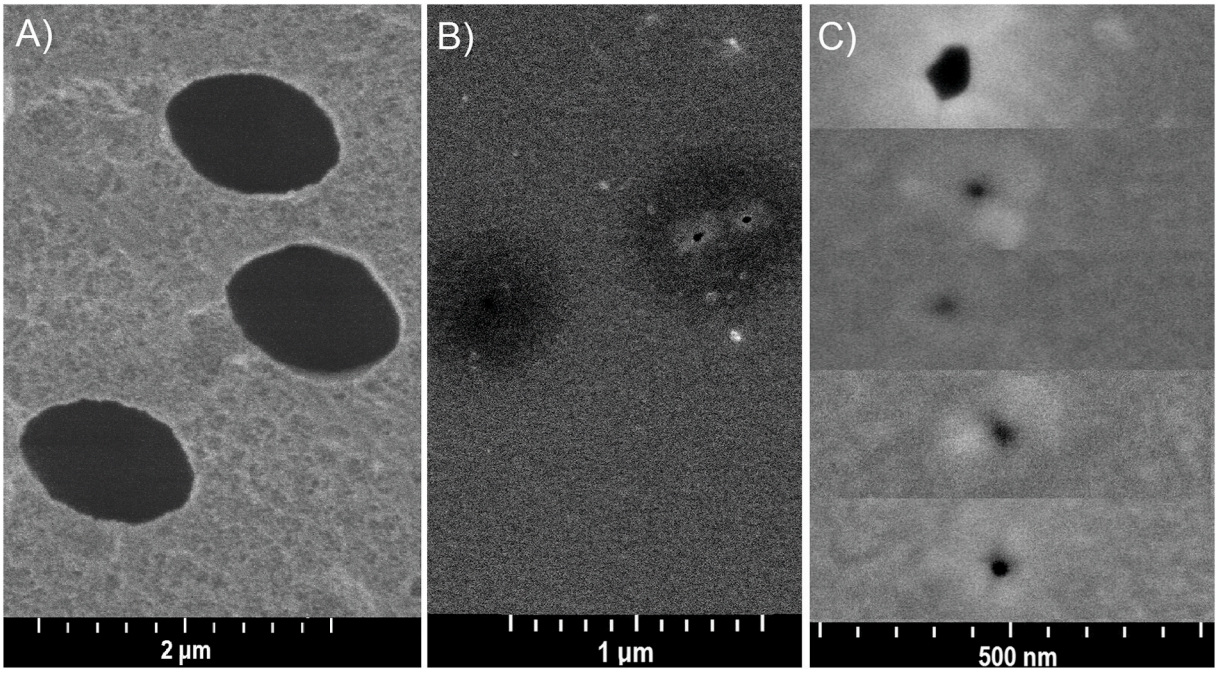

Fig. 6. FESEM photos of the two sides of a membrane etched asymmetrically in 9 M NaOH/water for 170 min. A: Large pore diameter side. B, C: Small pore diameter side. Image C is a collection of surface fragments that contain one pore each. Sample of Fig. 4A.

found in both cases. Let us assume that at the end of etching, the solution in the pore tips (which are limiting regions) was strongly diluted, and its viscosity was equal to that of water. Then, we can write [5].

$$Q = L_p \Delta P \tag{6}$$

$$Q_s = L_p(\sigma \Delta\Pi - \Delta P_s) \tag{7}$$

Here, L_p is the hydraulic permeability of the membrane, $\Delta\Pi$ is the osmotic pressure difference and σ is the reflection coefficient. The ideal osmotic pressure is calculated as $\Delta\Pi = i\Delta cRT$, where c is the molar concentration, R is the gas constant, T is the temperature and i is a coefficient that takes into account the dissociation of the solute.

Combining equations (6) and (7), we obtain

$$\sigma \Delta\Pi = \frac{\Delta P\, Q_s}{Q} + \Delta P_s \tag{8}$$

Equation (8) gives a value of 0.90 kPa for the quantity $\sigma\Delta\Pi$. The ideal osmotic pressure for the 9 M NaOH solution is equal to 44 MPa at room temperature. The resulting reflection coefficient is as small as $2{\cdot}10^{-5}$. This value is definitely underestimated, which is clear from the observation of osmotic flow in similar experiments at the solution level of ~ 100 mm [50], and therefore, $\Delta\sigma\,\Pi$ should be larger than 1.3 kPa. As the other extreme, we can assume that the solution in the pore has the viscosity of the 9 M NaOH solution, i.e., one order of magnitude higher than water [61]. In this case, the value of L_p in equation (7) is 10 times larger than that in equation (6), and the reflection coefficient will increase up to ~ $1.4{\cdot}10^{-4}$. This value is also very small, indicating that the osmotic flow develops due to the very large concentration difference and the low hydraulic resistance of the highly asymmetric membrane. At least partially, the value of the reflection coefficient is diminished by the external concentration polarization [50].

To gain further information on the fabricated ATEM, the sample was subjected to osmotic experiments with less concentrated electrolyte solutions. The experimental setup has been described in detail previously [57]. In contrast to etching experiments, solutions on both sides of the membrane were thoroughly stirred to exclude external concentration polarization. Two draw solutions – sodium dodecyl sulfate (SDS) and potassium sulfate – were used at a concentration of 4 mM. Fig. 7A shows the dynamics of osmotic flow for the two draw solutions and two different orientations of the membrane between the draw and feed compartments.

The solution level vs. time dependences, $h(t)$, were approximated using an exponential function, as has been executed in Ref. [57]:

$$h(t) = h_{max}\left[1 - e^{-t/\tau}\right] \tag{9}$$

Here $h_{\max}$ is the maximum solution level and the parameter τ depends on the capillary cross section S_c, the hydraulic permeability L_p, the acceleration of gravity g and the solution density ρ:

$$\tau = \frac{S_c}{L_p \rho\, g} \tag{10}$$

The extracted values of $h_{\max}$ and L_p are shown in Table 1.

The reflection coefficients σ for the four different experimental conditions were calculated using

$$\sigma = \frac{h_{max}\, g\, \rho}{\Delta\Pi} \tag{11}$$

In contrast to the concentrated alkali solution, the diluted draw solutions show appreciable values of the reflection coefficient, which indicates that the membrane possesses a noticeable ionic selectivity.

There is a remarkable difference between the osmotic effects with two different electrolytes. SDS, capable of adsorption, induces a lower flow rate but generates a higher osmotic pressure. Accordingly, the reflection coefficient for SDS is higher than that for K_2SO_4. This result is due to the formation of an adsorption layer of SDS, which presumably

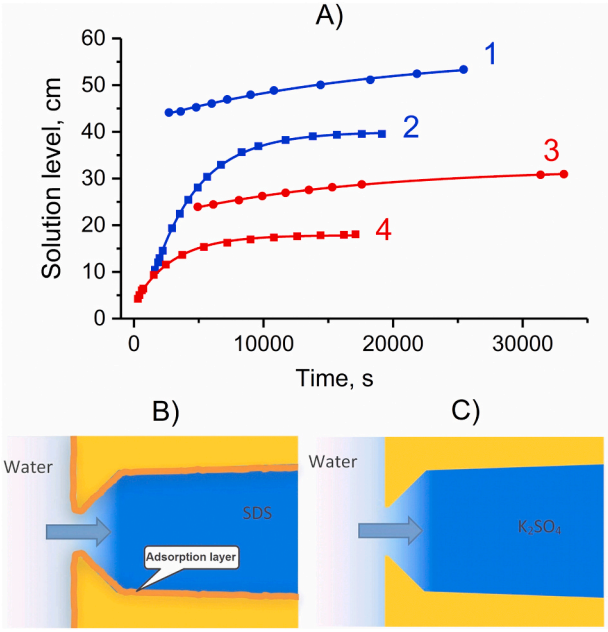

Fig. 7. A: The draw solution level as a function of time in osmotic experiments using 4 mM sodium dodecyl sulfate (1, 3) and 4 mM potassium sulfate (2, 4) as draw solutions and water as a feed solution. The membrane from the experiment of Fig. 4A. The large pore diameter side is exposed to the draw solution (1, 2) and to the feed solution (3, 4). The working surface area is 1 cm^2. B, C: Qualitative illustration of the effect of the surfactant on osmotic flow through a short channel. B and C correspond to curves 1 and 2, respectively.

Table 1
Asymmetric membrane characteristics calculated from the data of Fig. 7A.

Conditions	L_p, 10^{-15} m^3 Pa^{-1} s^{-1}	h_{max}, cm	$\Delta\Pi$, kPa	σ	Tip radius, nm
4 mM SDS, curve 1 in Fig. 7A	4.5 ± 0.6	56.8 ± 0.9	19.6	0.28	5.8
4 mM SDS, curve 3	5.6 ± 0.4	32.1 ± 0.2	19.6	0.16	
4 mM K_2SO_4, curve 2	22.6 ± 0.2	40.0 ± 0.2	29.5	0.13	9.8
4 mM K_2SO_4, curve 4	26.3 ± 0.8	17.8 ± 0.1	29.5	0.06	
Water flow under ΔP = 5 kPa	65 ± 3	–	–	–	13.5

increases the density of the negative charge on the pore walls and reduces the pore cross section [57]. Assuming that formula (2) is valid for the case of osmotic flow, the tip radii, $d/2$, were calculated from the membrane hydraulic permeabilities L_p, averaged for two different orientations (see the last column of Table 1). For the multipore membrane, formula (2) is transformed into

$$Q_{ap} = \frac{N\, d^3 \Delta P}{24\mu} \tag{12}$$

with $L_p = \frac{N\, d^3}{24\mu}$, where N is the number of pores in the membrane. The presence of SDS in the draw solution reduces the pore radius by 4 nm. This value is twice as large as the apparent thickness of the SDS adsorption layer found in similar experiments with long cylindrical pores [57]. The origin of this difference is not clear. A monolayer of SDS cannot be as thick as 4 nm, and a double layer of the anionic surfactant cannot form on the polymer surface [62]. Therefore, the question of such a considerable reduction in the effective pore cross section remains open. One can speculate that the osmotic flux through a short channel has a different velocity profile compared to that for the viscous flow

described by formula (12), which leads to overestimating the adsorption layer thickness.

The second noticeable feature is the difference between the permeability of the asymmetric membrane under the hydrostatic pressure and permeability found from osmotic flow. The latter is lower for both electrolytes used. Taking into account the FESEM data, one can suggest that some pores, most likely the largest ones, have a negligible reflection coefficient and do not contribute to the osmotic flow. In contrast, the largest pores contribute to the viscous flow under hydrostatic pressure. In other words, ΔP is a driving force applied to the whole membrane including the liquid in all pores, while $\Delta\Pi$ is a driving force that acts on the liquid only in pores with a nonzero reflection coefficient [63]. This behavior is why the "hydrostatic" pore tip radius is 13.5 nm and the "osmotic" pore tip radius is 9.8 nm. Using the "osmotic" pore radius, r_{os}, we calculate the linear velocity of the solution through the pore tip (averaged over the cross section) at the end of the experiment of Fig. 4A:

$$v = \frac{Q_s}{N\pi r_{os}^2} = 0.17 \text{ cm s}^{-1}$$

The third characteristic feature of the ATEM sample is the asymmetry of osmotic properties. For both electrolytes, the flux is higher when the large pore diameter side is exposed to the draw solution, as shown in Fig. 7B and C. This behavior is the opposite of that of typical forward osmosis asymmetric membranes, where internal polarization plays a decisive role [5]. In the case of our asymmetric channels, another mechanism plays the game. The ionic selectivity is higher when a diluted solution faces the small pore diameter side [64], and therefore, this configuration provides a larger reflection coefficient.

The fourth remarkable point is the difference between the reflection coefficients found for the ATEM sample and the membranes with long cylindrical nanopores with the same pore diameter (25 nm) [57]. The former are several times smaller, which can be related to the length of the nanochannels. A lower ionic selectivity of the short nanochannels with charged walls has been predicted theoretically [65]. As stated in Ref. [66], the selectivity of long pores is primarily determined by the low concentration side due to lack of electrostatic shielding of the charged surface. Unlike long pores, the selectivity of nanopores in 2D membranes is determined by the Debye length on the high concentration side.

Finally, the formula for the conical geometry was tested for applicability to such asymmetric pores. For small cone angles, the following expression can be used [67]:

$$Q = \frac{3\pi N r_t^4 \Delta P}{8\mu L f} \tag{13}$$

Here, $f = r_t/R + \left(r_t/R\right)^2 + \left(r_t/R\right)^3$, r_t and R are the tip and base radii. Taking into account that the difference between r_t and R is nearly two orders of magnitude, the formula can be transformed into

$$Q = \frac{3\pi N {r_t}^3 R \Delta P}{8\mu L} \tag{14}$$

The geometrical mean of the ellipse axes of the apertures shown in Fig. 6A was used to obtain $R = 0.515$ μm. For a hydraulic permeability of $6.5{\cdot}10^{-14}$ m^3 Pa^{-1} s^{-1}, formula (14) yields the tip radius in the conical approximation

$$r_t = 25 \text{ nm},$$

which is evidently unrealistic. FESEM images show that the average size of the pore openings is much smaller.

3.5. Use of the results in the field

The results of this study distinguish between several consecutive phases of pore shape transformations and identify the causative relationships behind these transformations. Understanding the physical and chemical processes that govern the pore shape and its transport properties is important with regard to the characterization of asymmetric nanopores using any direct or indirect method. SEM observations of nanopore replicas in the form of nanowires and sample fractures are widely used in practice [39,68–78]. However, the imaged tapered nanowires or longitudinal sections of channels correspond to different and often unknown stages of pore evolution. This effect especially applies to the etching of multipore samples where the breakthrough time of an individual pore channel cannot be measured. Our results may help to correlate the nanowire shape and the age of the relevant pore after its breakthrough. In many of the studies, the observed pores belong to stage III of their evolution, when they have already deviated from the original quasi-conical shape [39,74,76,77]. Replicas corresponding to both stages II and III are presented in Refs. [69,70,72,75]. The moment when a pore was actually very close to the conical shape was captured in Refs. [71,73]. Good images illustrating stage I are quite rare [75,78].

Note that all the above conclusions on the pore evolution are valid for asymmetric etching in the absence of a bias voltage. The ionic current generated by an applied voltage should inevitably affect the ionic and water transport in asymmetric track-etched nanopores [68,69]. This fact should be kept in mind when the results for multitrack etching are applied to single-track etching with conductometric monitoring, and vice versa.

Based on the previously published data and the results of the present work, we can summarize the existing knowledge of asymmetric track etching, with an emphasis on single pores. Fig. 8 illustrates different scenarios that can be realized to fabricate a nanopore of a certain geometry in a PET foil. Image (A) presents a funnel-shaped pore just after breakthrough. Its narrow tip is surrounded by a track halo consisting of a cross-linked polymer. Image (B) shows the evolution of the pore when asymmetric etching continues after breakthrough at the same bias voltage. The electric field effectively extracts hydroxide ions from the pore tip, and its size and shape are nearly "frozen". In the wide part of the pore, the strength of the electric field is several orders of magnitude lower. Therefore, the alkali concentration in this region is supported by diffusion, and the radius of the base continues to grow. The ionic current through the pore develops very slowly because the widening of the base weakly affects the pore resistance and the tip radius only changes slightly. The resulting pore shows a moderate rectification effect, but its shape is not conical. Rather, a funnel-like shape is accentuated, which is especially pronounced at higher bias voltages [68]. Image (C) shows the case when the polarity of the bias voltage is reversed after breakthrough. The electric field induces homogeneous filling of the pore with hydroxide ions. Applying the Huygens principle to the track etching process [79], the pore evolution can be regarded as a movement of the pore profile from right to left, and the pore gradually acquires a conical geometry. The time needed for achieving the conical shape can be found from diagrams presented in Ref. [80]. For track-forming ions as heavy as Au or U, the elongated region surrounded by the track halo should be completely removed in ~10 min, and the tip radius will increase up to 15–20 nm. For lighter ions such as Kr or Fe, the track halo is narrower, and the pores acquire a conical shape much sooner. The ionic current through the pore grows rapidly [47], which impedes the accurate monitoring of pore evolution. Image (D) shows the approach suggested in Ref. [73], which was successfully used, for instance, in Ref. [39]. After breakthrough, the etchant and stopping solutions are replaced with a new, more diluted, alkali solution. Further etching proceeds under symmetric conditions, thus, the polarity of the bias voltage does not matter. The pore develops in a manner similar to case (C) but less rapidly. Therefore, it is more convenient to monitor the pore evolution by measuring the ionic current and stopping the etching process at the right moment. Unlike the two previous cases, the bulk value of the specific conductivity k of the etchant is valid for the inner pore volume. After the pore attains a conical geometry, its tip and base radii can be correctly calculated from the electrical conductivity G using the well-known formula:

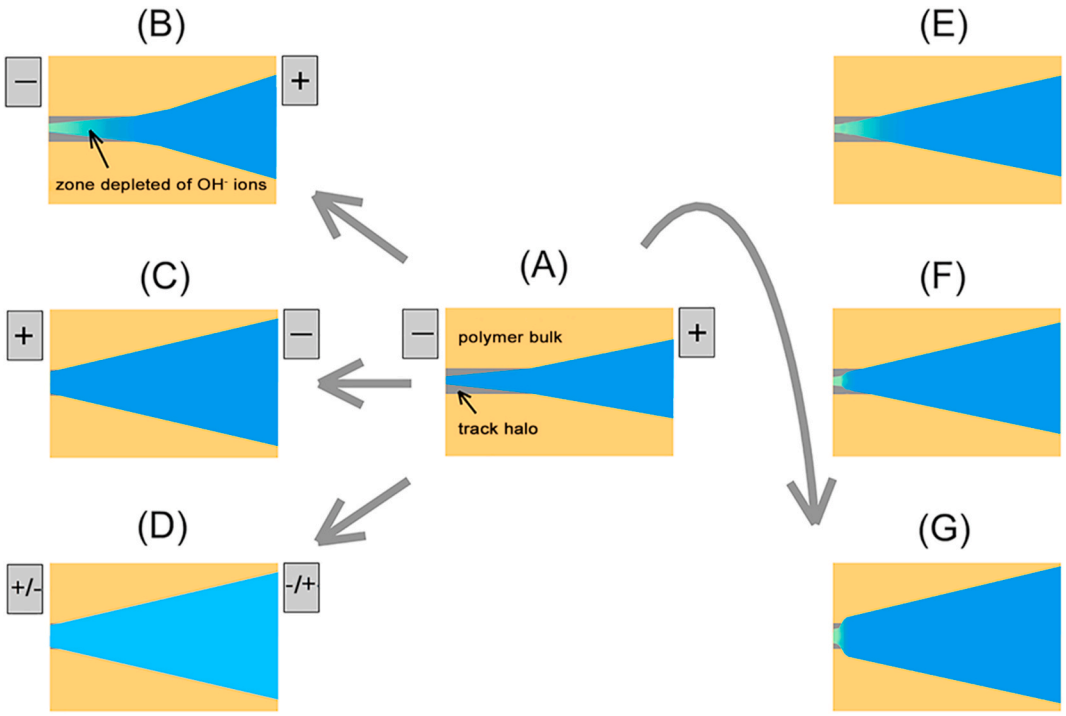

Fig. 8. Different scenarios of asymmetric single-pore etching continued after breakthrough. (A) Pore geometry at the moment of breakthrough. A positive bias voltage is applied to the base side. (B) Asymmetric etching continues at the same bias voltage. (C) Asymmetric etching continues, and the polarity of the bias voltage is reversed. (D) Symmetric etching with a diluted alkali solution. (E, F, G) Asymmetric etching continues with no bias voltage. The etching time increases from E to G. The intensity of the blue color is proportional to the concentration of hydroxide ions.

$$G = \frac{k\pi r_t R}{L} \quad , \tag{15}$$

Case (D) can also be realized with the same highly concentrated alkali solution (9 M NaOH) on both sides of the membrane [49]. Using the algorithm developed in Refs. [49, 80], the electrical conductivity vs. time function can be converted into the profile $r(x)$ which the pore possessed at the breakthrough moment. Images (E-G) illustrate the pore etching process after breakthrough under asymmetric conditions in the absence of a bias voltage. Due to a sharp alkali concentration gradient in the tip region (see equation (5)), the very tip grows extremely slowly. The wide conical part of the pore, filled with the etchant of a nearly constant concentration, moves from right to left. The speed of the virtual movement of the cone is equal to the foil thickness divided by the breakthrough time. At a particular moment, the pore acquires an approximately conical shape as shown in image (E). Note that the tip radius of the cone will be smaller compared to cases (C) and (D). Further, the conical part continues to move toward the tip while the tip remains small. The transition region between the tip and the cone is gradually compressed, which results in the configurations shown in (F) and (G). Typical SEM images illustrating this process are presented in Ref. [50].

Traditionally, asymmetric track etching is considered a method for the fabrication of conical pores. The above analysis shows that this method has wide potential for use in the controlled production of a variety of pore shapes, including a structure that resembles a 2D porous material. Moreover, the method can be applied to existing (pre-etched) pores to overcome the problem of the wide dispersion of pore radii in selective layers [50].

4. Conclusions

We applied four experimental methods to disentangle the contributions of diffusion and osmotic effects to the geometrical evolution of pore channels in asymmetric track-etched membranes. It is found that a newborn track-etched pore has a high hydraulic resistance and does not generate osmotic flow, contrary to the suggestion made in Refs. [49,50]. In the next stage of etching, the shape of the pore changes because of the nonlinearity of the diffusion-controlled etchant concentration gradient. The pore channel widens except for the pore tip, which remains narrow, typically ranging from several nanometers to ~10 nm in radius. In the late stage of etching, the pore strongly deviates from the original approximately conical geometry. The narrow ends of the pores are rounded, and the very tips constitute short channels in the pore bottoms. Permeability measurements – both under a hydraulic pressure difference and an osmotic pressure difference – showed that the converging flow into the channel entrance and the diverging flow out of the channel determine the total resistance of the highly asymmetric pores. Thus, the fabricated membrane with a thin selective layer provides conditions for osmotic flow. In particular, on the one hand, the pore has a relatively low hydraulic resistance; on the other hand, the pore tip is sufficiently narrow to have a nonzero reflection coefficient.

The osmotic reflection coefficient of $\sim 10^{-4}$ was found for a membrane in the late stage of etching. The low value of σ is expected because of the small thickness of the electrical double layer in the concentrated etching solution. In the diluted electrolyte solutions ($\sim 10^{-3}$ mol/L), a clear asymmetry of osmotic properties is observed, and the reflection coefficient increases up to (0.1–0.3), which indicates a moderate ionic selectivity of nanopores in the fabricated highly asymmetric membranes.

Our results allowed us to achieve a new level of understanding of the phenomena underlying the development of an ion-track nanopore. First, this understanding is of primary importance for the improvement in the metrology of the objects of this kind. Second, detailed knowledge of pore evolution under asymmetric etching conditions may help to develop new approaches for the designed fabrication of single- and multi-nanopore membranes with desired properties.

CRediT author statement

I.V. Blonskaya: Investigation, Methodology, Formal analysis.
N.E. Lizunov: Investigation.
K. Olejniczak: Resources, Investigation, Writing- Reviewing and Editing.
O.L. Orelovich: Methodology, Investigation.
Y. Yamauchi: Investigation, Formal analysis.
M.E. Toimil-Molares: Resources, Methodology, Writing- Reviewing and Editing.
C. Trautmann: Resources, Methodology.
P.Y. Apel: Conceptualization, Formal analysis, Writing - Original Draft, Writing- Reviewing and Editing.

Declaration of competing interest

The authors declare that they have no known competing financial interests or personal relationships that could have appeared to influence the work reported in this paper.

Acknowledgements

This work was partially supported by the Polish Government Plenipotentiary for JINR in Dubna (grant numbers 104/18/2019 and 129/49/2019).

References

[1] R.J. Petersen, Composite reverse osmosis and nanofiltration membranes, J. Membr. Sci. 83 (1993) 81–150.
[2] R.M. Boom, I.M. Wienk, Th. van den Boomgaard, C.A. Smolders, Microstructures in phase inversion membranes. Part 2. The role of a polymeric additive, J. Membr. Sci. 73 (1992) 277–292.
[3] L. Eykens, K. De Sitter, C. Dotremont, L. Pinoy, D. Van der Bruggen, Membrane synthesis for membrane distillation: a review, Sep. Purif, Technol. 182 (2017) 36–51.
[4] M. Ulbricht, O. Schuster, W. Ansorge, M. Ruetering, P. Steiger, Influence of the strongly anisotropic cross-section morphology of a novel polyethersulfone microfiltration membrane on filtration performance, Sep. Purif. Technol. 57 (2007) 63–73.
[5] T.Y. Cath, A.E. Childress, M. Elimelech, Forward osmosis: principles, applications, and recent developments, J. Membr. Sci. 281 (2006) 70–87.
[6] R. van Reis, A. Zydney, Bioprocess membrane technology, J. Membr. Sci. 297 (2007) 16–50.
[7] M. Mireles, T.R. Gaborski, Fabrication techniques enabling ultrathin nanostructured membranes for separations, Electrophoresis 38 (2017) 2374–2388.
[8] J. Wang, D.S. Dlamini, A.K. Mishra, M.T.M. Pendergast, M.C.Y. Wong, B.B. Mamba, V. Freger, A.R.D. Verliefde, E.M.V. Hoek, A critical review of transport through osmotic membranes,, J. Membr. Sci. 454 (2014) 516–537.
[9] C. Algieri, E. Drioli, L. Guzzo, L. Donato, Bio-mimetic sensors based on molecularly imprinted membranes, Sensors 14 (2014) 13863–13912.
[10] S. Howorka, Z. Siwy, Nanopore analytics: sensing of single molecules, Chem. Soc. Rev. 38 (2009) 2360–2380.
[11] W. Shi, A.K. Friedman, L.A. Baker, Nanopore sensing, Anal. Chem. 89 (2017) 157–188.
[12] J.J. Kasianowicz, E. Brandin, D. Branton, D.W. Deamer, Characterization of individual polynucleotide molecules using a membrane channel, Proc. Natl. Acad. Sci. Unit. States Am. 93 (1996) 13770–13773.
[13] I.M. Derrington, T.Z. Butler, M.D. Collins, E. Manrao, M. Pavlenok, M. Niederweis, J.H. Gundlach, Nanopore DNA sequencing with MspA, Proc. Natl. Acad. Sci. Unit. States Am. 107 (2010) 16060–16065.
[14] C. Cao, Y.-L. Ying, Z.-L. Hu, D.-F. Liao, H. Tian, Y.-T. Long, Discrimination of oligonucleotides of different lengths with a wild-type aerolysin nanopore, Nat. Nanotechnol. 11 (2016) 713–718.
[15] J. Li, M. Gershow, D. Stein, E. Brandin, J.A. Golovchenko, DNA molecules and configurations in a solid-state nanopore microscope, Nat. Mater. 2 (2003) 611–615.
[16] H. Chang, F. Kosari, G. Andreadakis, M.A. Alam, G. Vasmatzis, R. Bashir, DNA-mediated fluctuations in ionic current through silicon oxide nanopore channels, Nano Lett. 4 (2004) 1551–1556.
[17] G.F. Schneider, S.W. Kowalczyk, V.E. Calado, G. Pandraud, H.W. Zandbergen, L.M. K. Vandersypen, C. Dekker, DNA translocation through graphene nanopores, Nano Lett. 10 (2010) 3163–3167.
[18] J. Feng, K. Liu, R.D. Bulushev, S. Khlybov, D. Dumcenco, A. Kis, A. Radenovic, Identification of single nucleotides in MoS_2 nanopores, Nat. Nanotechnol. 10 (2015) 1070–1076.
[19] M.A. Shehzad, Y. Wang, A. Yasmin, X. Ge, Y. He, X. Liang, Y. Zhu, M. Hu, X. Xiao, L. Ge, C. Jiang, Z. Yang, M.D. Guiver, L. Wu, T. Xu, Biomimetic nanocones that enable high ion permselectivity, Angew. Chem. 131 (2019) 2–11.
[20] J. Li, D. Stein, C. McMullan, D. Branton, M.J. Aziz, J.A. Golovchenko, Ion-beam sculpting at nanometre length scales, Nature 412 (2001) 166–169.
[21] A.J. Storm, J.H. Chen, X.S. Ling, H.W. Zandbergen, C. Dekker, Fabrication of solid-state nanopores with single-nanometre precision, Nat. Mater. 2 (2003) 537–540.
[22] J. Feng, K. Liu, M. Graf, M. Lihter, R.D. Bulushev, D. Dumcenco, D.T.L. Alexander, D. Krasnozhon, T. Vuletic, A. Kis, A. Radenovic, Electrochemical reaction in single layer MoS_2: nanopores opened atom by atom, Nano Lett. 15 (2015) 3431–3438.
[23] P. Apel, Track etching technique in membrane technology, Radiat. Meas. 34 (2001) 559–566.
[24] T. Ma, J.-M. Janot, S. Balme, Track-etched nanopore/membrane: from fundamental to applications, Small Meth (2020), https://doi.org/10.1002/smtd.202000366.
[25] P. Wang, M. Wang, F. Liu, S. Ding, X. Wang, G. Du, J. Liu, P. Apel, P. Kluth, C. Trautmann, Y. Wang, Ultrafast ion sieving using nanoporous polymeric membranes, Nat. Commun. 9 (2018) 569.
[26] A.R. Hall, A. Scott, D. Rotem, K.K. Mehta, H. Bayley, C. Dekker, Hybrid pore formation by directed insertion of α-haemolysin into solid-state nanopores, Nat. Nanotechnol. 5 (2010) 874–877.
[27] Y. Zhao, C. Qiu, X. Li, A. Vararattanavech, W. Shen, J. Torres, C.H. Lix-Nielsen, R. Wang, X. Hu, A.G. Fan, C.Y. Tang, Synthesis of robust and high-performance aquaporin-based biomimetic membranes by interfacial polymerization-membrane preparation and RO performance characterization, J. Membr. Sci. 423–424 (2012) 422–428.
[28] Y. Shen, P.O. Saboe, I.T. Sines, M. Erbakan, M. Kumar, Biomimetic membranes: a review, J. Membr. Sci. 454 (2014) 359–381.
[29] P.Yu. Apel, I.V. Blonskaya, S.N. Dmitriev, T.I. Mamonova, O.L. Orelovitch, B. Sartowska, Yu. Yamauchi, Surfactant-controlled etching of ion track nanopores and its practical applications in membrane technology, Radiat. Meas. 43 (2008) 552–559.
[30] P.Y. Apel, Fabrication of functional micro- and nanoporous materials from polymers modified by swift heavy ions, Radiat. Phys. Chem. 159 (2019) 25–34.
[31] R. Spohr, Status of ion track technology – prospects of single tracks, Radiat. Meas. 40 (2005) 191–202.
[32] B. Schiedt, K. Healy, A.P. Morrison, R. Neumann, Z. Siwy, Transport of ions and biomolecules through single asymmetric nanopores in polymer films, Nucl. Instrum. Methods Phys. Res. B 236 (2005) 109–116.
[33] J. Cervera, B. Schiedt, R. Neumann, S. Mafe, P. Ramirez, Ionic conduction, rectification, and selectivity in single conical nanopores, J. Chem. Phys. 124 (2006) 104706.
[34] J. Cervera, A. Alcaraz, B. Schiedt, R. Neumann, P. Ramirez, Asymmetric selectivity of synthetic conical nanopores probed by reversal potential, J. Phys. Chem. C 111 (2007) 12265–12273.
[35] Y. Choi, L.A. Baker, H. Hillebrenner, C.R. Martin, Biosensing with conically shaped nanopores and nanotubes, Phys. Chem. Chem. Phys. 8 (2006) 4976–4988.
[36] I. Vlassiouk, T.R. Kozel, Z.S. Siwy, Biosensing with nanofluidic diodes, J. Am. Chem. Soc. 131 (2009) 8211–8220.
[37] M. Lepoitevin, T. Ma, M. Bechelany, J.-M. Janot, S. Balme, Functionalization of single solid state nanopores to mimic biological ion channels: a review. Adv, Colloid Interface Sci. 250 (2017) 195–213.
[38] E.A. Heins, Z. Siwy, L.A. Baker, C.R. Martin, Detecting single porphyrin molecule in a conically shaped synthetic nanopore, Nano Lett. 5 (2005) 1824–1829.
[39] L.T. Sexton, L.P. Horne, S.A. Sherrill, G.W. Bishop, L.A. Baker, C.R. Martin, Resistive-pulse studies of proteins and protein/antibody complexes using a conical nanotube sensor, J. Am. Chem. Soc. 129 (2007) 13144–13152.
[40] G. Pérez-Mitta, A.S. Peinetti, M.L. Cortez, M.E. Toimil-Molares, C. Trautmann, O. Azzaroni, Highly sensitive biosensing with solid-state nanopores displaying enzymatically reconfigurable rectification properties, Nano Lett. 18 (2018) 3303–3310.
[41] S.F. Buchsbaum, G. Nguyen, S. Howorka, Z.S. Siwy, DNA-modified polymer pores allow pH- and voltage-gated control of channel flux, J. Am. Chem. Soc. 136 (2014) 9902–9905.
[42] J. Cervera, P. Ramirez, V. Gomez, S. Nasir, M. Ali, W. Ensinger, P. Stroeve, S. Mafe, Multipore membranes with nanofluidic diodes allowing multifunctional rectification and logical responses, Appl. Phys. Lett. 108 (2016) 253701.
[43] X. Wu, P.R. Rajasekaran, C.R. Martin, An alternating current electroosmotic pump based on conical nanopore membranes, ACS Nano 10 (2016) 4637–4643.
[44] M. Ali, S. Mafe, P. Ramirez, R. Neumann, W. Ensinger, Logic gates using nanofluidic diodes based on conical nanopores functionalized with polyprotic acid chains, Langmuir 25 (2009) 11993–11997.
[45] J. Lu, H. Zhang, J. Hou, X. Li, X. Hu, Y. Hu, C.D. Easton, Q. Li, C. Sun, A. W. Thornton, M.R. Hill, X. Zhang, G. Jiang, J.Z. Liu, A.J. Hill, B.D. Freeman, L. Jiang, H. Wang, Efficient metal ion sieving in rectifying subnanochannels enabled by metal–organic frameworks, Nat, Mater (2020) 767–774, https://doi.org/10.1038/s41563-020-0634-7.
[46] G. Laucirica, A.G. Albesa, M.E. Toimil-Molares, C. Trautmann, W.A. Marmisollé, O. Azzaroni, Shape matters: enhanced osmotic energy harvesting in bullet-shaped nanochannels, Nano Energy 71 (2020) 104612.
[47] P.Yu. Apel, Yu.E. Korchev, Z. Siwy, R. Spohr, M. Yoshida, Diode-like single-ion track membrane prepared by electro-stopping, Nucl. Instrum. Meth.. in Phys. Res. B 184 (2001) 337–346.
[48] P.Y. Apel, I.V. Blonskaya, S. Dmitriev, O.L. Orelovitch, A. Presz, B.A. Sartowska, Fabrication of nanopores in polymer foils with surfactant-controlled longitudinal profile, Nanotechnology 18 (2007) 305302.

[49] P.Y. Apel, V.V. Bashevoy, I.V. Blonskaya, N.E. Lizunov, O.L. Orelovitch, C. Trautmann, Shedding light on the mechanism of asymmetric track etching: an interplay between latent track structure, etchant diffusion and osmotic flow, Phys. Chem. Chem. Phys. 18 (2016) 25421–25433.
[50] P.Y. Apel, I.V. Blonskaya, N.E. Lizunov, K. Olejniczak, O.L. Orelovitch, M.E. Toimil-Molares, C. Trautmann, Osmotic effects in track-etched nanopores, Small 14 (2018) 1703327.
[51] J.F. Ziegler, J.P. Biersack, U. Littmark, The Stopping and Range of Ions in Solids, Pergamon, New York, 1985. Free SRIM software is available from the website, http://www.srim.org.
[52] G. Åkerlöf, G. Kegeles, The density of aqueous solutions of sodium hydroxide, J. Am. Chem. Soc. 62 (1940) 620–638.
[53] A. Schulz, M. Danziger, G.N. Akapjev, V.V. Trofimov, K. Prokert, The pore-opening process of etching PETP films irradiated by multiple heavy ions and the three-phase model of etching process of the single ion track, in: YuTs Oganessian, R. Kolpakchieva (Eds.), Heavy Ion Physics (VI Intern. School-Seminar, Dubna, September 22-27, 1997), World Scientific, Singapore, 1998, pp. 792–795.
[54] D. Fink, S. Ghosh, K. Hirata, R. Klett, K.K. Dwivedi, J. Vacik, V. Hnatowicz, On the interaction of penetrant solutions with pristine and ion-irradiated polyimide, in: YuTs Oganessian, R. Kolpakchieva (Eds.), Heavy Ion Physics (VI Intern. School-Seminar, Dubna, September 22-27, 1997, World Scientific, Singapore, 1998, pp. 792–795.
[55] D. Fink, G.M. Hernandez, S.A. Cruz, H. Garcia-Arellano, J. Vacik, V. Hnatowicz, A. Kiv, L. Alfonta, Ion track etching revisited: II. Electronic properties of aged tracks in polymers, Radiat. Eff. Defect Solid 173 (2018) 148–164.
[56] P.Y. Apel, I.V. Blonskaya, O.M. Ivanov, O.V. Kristavchuk, N.E. Lizunov, A. N. Nechaev, O.L. Orelovich, O.A. Polezhaeva, S.N. Dmitriev, Creation of ion-selective membranes from polyethylene terephthalate films irradiated with heavy ions: critical parameters of the process, Membr. Membr. Technol 2 (2020) 98–108.
[57] Y. Yamauchi, I.V. Blonskaya, P. Yu, Apel, Osmosis in negatively charged nanocapillaries and its enhancement by an anionic surfactant, Colloid J. 80 (2018) 792–802.
[58] K. Olejniczak, O.L. Orelovich, P.Y. Apel, Variation in geometry and electrical conductance properties of asymmetric track-etched single nanopores: how uniform are they? Nucl. Instrum. Meth.. in Phys. Res. B 365 (2015) 646–650.
[59] J. Happel, H. Brenner, Low Raynolds Number Hydrodynamics with Specialapplications to Particulate Media, Prentice-Hall, Englewood Cliffs, NJ, 1965.
[60] R. Roscoe, XXXI. The flow of viscous fluids round plane obstacles, The London, Edinburgh, and Dublin Philosophical Magazine and Journal of Science 40 (Series 7) (1949) 338–351.
[61] J. D'Ans, E. Lax, Taschenbuch für Chemiker und Physiker, Springer-Verlag, Berlin Heidelberg, 1943.
[62] P.D. Bisio, J.G. Cartledge, W.H. Keesom, C.J. Radke, Molecular orientation of aqueous surfactants on a hydrophobic solid, J. Colloid Interface Sci. 78 (1980) 225–234.
[63] J.G. Wijmans, R.W. Baker, The solution-diffusion model: a review, J. Membr. Sci. 107 (1995) 1–21.
[64] Z. Siwy, I.D. Kosinska, A. Fulinski, C.R. Martin, Asymmetric diffusion through synthetic nanopores, Phys. Rev. Lett. 94 (2005) 48102.
[65] I. Vlassiouk, S. Smirnov, Z. Siwy, Ionic selectivity of single nanochannels, Nano Lett. 8 (2008) 1978–1985.
[66] S. Sahu, M. Zwolak, Colloquium: ionic phenomena in nanoscale pores through 2D materials, Rev. Mod. Phys. 91 (2019) 21004.
[67] G.M. Gusinskii, E.B. Kremer, M.I. Kremer, B.V. Mchedlishvili, Determination of the size of micropores in nuclear microfilters with small diameter, J. Eng. Phys. 37 (1979) 1493–1496.
[68] C.C. Harrell, Z.S. Siwy, C.R. Martin, Conical nanopore membranes: controlling the nanopore shape, Small 2 (2006) 194–198.
[69] F. Roustaie, J. Bieker, R. Cicek, H.F. Schlaak, Novel fabrication method for integration of template grown metallic nanocones with controllable tip diameter and apex angle, Microelectron. Eng. 180 (2017) 81–85.
[70] I. Enculescu, Z. Siwy, D. Dobrev, C. Trautmann, M.E. Toimil-Molares, R. Neumann, K. Hjort, L. Westerberg, R. Spohr, Copper nanowires electrodeposited in etched single-ion track templates, Appl. Phys A 77 (2003) 751–755.
[71] P. Scopece, L.A. Baker, P. Ugo, C.R. Martin, Conical nanopore membranes: solvent shaping of nanopores, Nanotechnology 17 (2006) 3951–3956.
[72] I. Enculescu, Nanowires and nanotubes prepared using ion track membranes as template, J. Nanomater. Biostruct 1 (2006) 15–20.
[73] J.E. Wharton, P. Jin, L.T. Sexton, L.P. Horne, S.A. Sherrill, W.K. Mino, C. Martin, A method for reproducibly preparing synthetic nanopores for resistive-pulse biosensors,, Small 3 (2007) 1424–1430.
[74] W. Guo, J. Xue, L. Wang, Y. Wang, Controllable etching of heavy ion tracks with organic solvent addition in etchant, Nucl. Instrum. Meth.. In Phys. Res. B 266 (2008) 3095–3099.
[75] H. Mukaibo, L.P. Horne, D. Park, C.R. Martin, Controlling the length of conical pores etched in ion-tracked poly(ethylene terephthalate) membranes, Small 5 (2009) 2474–2479.
[76] G. Pérez-Mitta, L. Burr, J.S. Tuninetti, C. Trautmann, M.E. Toimil-Molares, O. Azzaroni, Noncovalent functionalization of solid-state nanopores via self-assembly of amphipols, Nanoscale 8 (2016) 1470–1478.
[77] G. Pérez-Mitta, W.A. Marmisolle, L. Burr, M.E. Toimil-Molares, C. Trautmann, O. Azzaroni, Proton-gated rectification regimes in nanofluidic diodes switched by chemical effectors, Small 14 (2018) 1703144.
[78] D.A. Cherkasov, D.V. Panov, I.M. Doludenko, V.M. Kanevskiy, A.E. Muslimov, D. L. Zagorskiy, D.A. Biziaev, A.A. Bukharaev, Microscopy investigation of conical and layered nanowires, IOP Conf. Ser: Mater. Sci. Eng. 699 (2019) 12005.
[79] R. Spohr, Ion Tracks and Microtechnology – Principles and Applications, Vieweg, Braunschweig, 1990.
[80] P.Y. Apel, P. Ramirez, I.V. Blonskaya, O.L. Orelovitch, B.A. Sartowska, Accurate characterization of single track-etched, conical nanopores, Phys. Chem. Chem. Phys. 16 (2014) 15214–15223.